Mixed mode fatigue crack propagation behaviour of aluminium F357 alloy

Abstract

Manufacturing defects are often not in the plane perpendicular to the loading direction and will propagate under mixed mode fatigue loading condition. This paper presents a numerical study of mixed mode crack growth behaviour in H-shaped specimens made of aluminium F357 alloy. The size and orientations of the crack are based on the fractographic observation of defects in F357 specimens manufactured by foundry. Equivalent values of the stress intensity factor (SIF) and the maximum circumferential tensile stress criterion have been adopted to simulate growth of cracks at angles of 90^{o}, 60^{o} and 45^{o} to the loading direction, respectively. Mixed mode fatigue crack growth behaviours are analysed in terms of the shape of crack front, SIF variation, and kink angle. The mixity of SIFs of three modes is complex at early stage of growth with the maximum mode III SIF value at the two ends and the maximum mode II SIF value at the middle of the crack front. The crack surface rotates during the mixed mode crack growth, becoming normal to the loading direction regardless of the initial orientation of the crack. The simulated crack front agrees well with the final elliptical shape of the crack front observed in the physical test specimens. The initial crack orientated at 45° to the loading direction has the longest fatigue life compared with other two crack orientations.

Keywords: Mixed-mode fatigue and fracture, Linear Elastic Fracture Mechanics (LEFM), Fatigue crack growth.

1. Introduction

A wide range of defects such as inclusions and porosities exist in foundry aluminium components which promote crack nucleation and significantly reduce the fatigue life of the component [1-4]. Inclusions are mainly due to the presence of slags [5], among which the most common ones are those due to the presence of the Al_2O_3 oxide [6, 7], and other complex oxides (MgO and $MgAl_2O_4$) [8]. Porosities are caused by hydrogen dissolved in the liquid metal through reactions between water vapour and aluminium itself [8]. The fatigue life of a defect is dependent on its size and orientation to the loading direction. For a crack not perpendicular to the loading direction, the interaction of the three fracture modes affects not only the equivalent SIF range but also the crack path and the shape of the crack front.

The interaction among the three modes is material dependent and needs to be studied for each individual material to characterise its mechanical performance. Defects in aluminium F357 alloy manufactured by foundry have difference orientations and are often subject to mixed mode loading conditions. It is however found that no research has been reported in literature on mixed mode fatigue crack growth of the aluminium F357 alloy. This paper fills the gap by presenting numerical results of mixed mode fatigue crack growth behaviour of the H-shaped specimens made of F357 aluminium alloy. The mixed mode condition was simulated based on the fractographic observations of the fracture surfaces of the F357 aluminium alloy.

2. Fractography

The fatigue behaviour is affected by their distribution, position, size and shape of the defects. L. Dietrich and J. Radziejewska [9] underlined that different types of defects distribution and shape affected the damage mechanisms and therefore the fatigue life of the component.

In order to identify the main source of crack in the specimens, SEM analysis have been carried out on the fracture surfaces of the F357 aluminium alloy specimens, for which the chemical composition is reported in table 1.

Table 1 – Chemical composition (wt %) of the F357 aluminium alloy.

Alloy	Al	Cu	Si	Zn	Mg	Fe	Mn	Ti	Be
F357	Bal	0.2	6.5-7.5	0.1	0.25-0.45	0.2	0.1	0.1	0.002

As an example, two pictures showing the **Subsurface defect** (Figure 1A) and the internal defect (Figure 1B) in the tested specimens are shown.

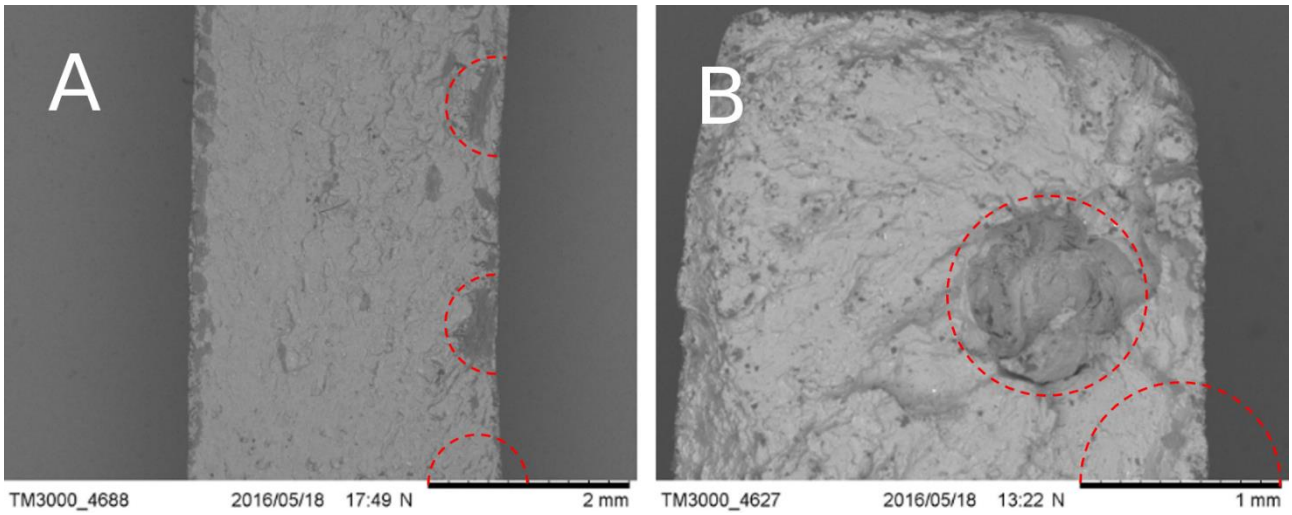

Figure 1 – SEM images taken from the specimens tested under fatigue. A) Subsurface defect B) internal defect.

The aim of the present work is to analyse the influence of the position and size of defects on crack growth behaviour in Aluminium F357 alloy specimens with an H-shaped geometry. The implementation of the numerical model was performed on the basis of experimental evidences collected through an experimental test campaign. The specimens were foundry manufactured by Augusta Westland. Axial fatigue tests were performed with a load ratio of R = 0.1 at a frequency of 10 Hz. During the fatigue test, each specimen was subject to an alternate tensile load with a maximum load value equal to P_{max} = 84.4 KN [10].

On the basis of the fractographic analysis carried out on the specimens tested under fatigue an initial defect having a dimension equal to 1 mm was chosen in order to consider the worst case scenario.

3. Numerical Modelling

3.1 Remeshing technique

A finite element model of a cracked H-shaped specimen was implemented through the use of a commercial code FRANC3D®, which allowed to deal with the insertion of the cracks in the uncracked model by means of the remeshing technique [11]. The remeshing technique consists of discretizing the continuous propagation phenomenon in a finite number of crack growth steps. For each step a FE model with a crack made up of two free surfaces in contact is implemented. This approach makes possible to determine the SIF values along the front. On the basis of such information it is possible to propagate the crack and create a new mesh with the new crack.

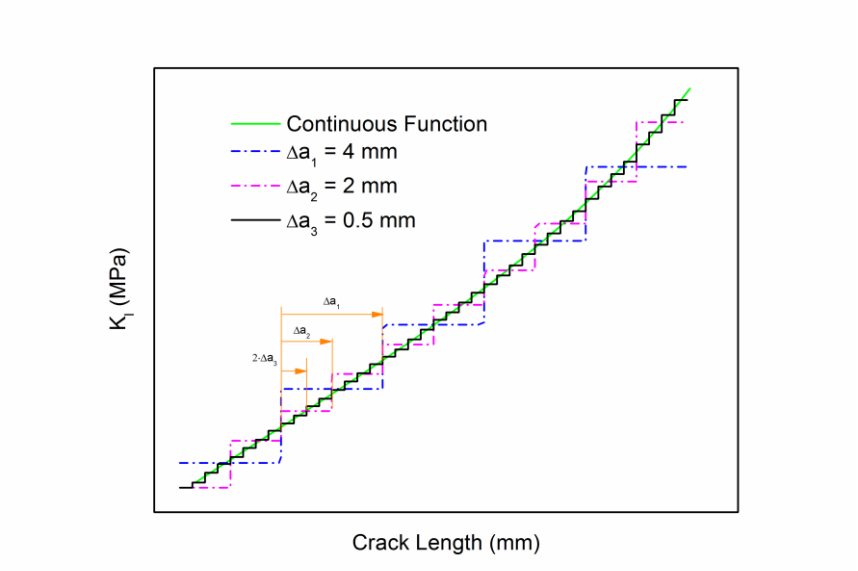

Figure 2 - Discretization of the continuous FCG process

The discretization of the continuous process in the remeshing technique introduces an error which depends on the chosen number of steps. In fact, by imposing a particular value of Δa the SIF value used to evaluate the progress is assumed to be a constant during each step of a certain number of cycles (Fig. 2). When the size of the Δa interval decreases, the constant value of the ΔK will be more representative. In order to determine the optimal Δa value considering both the accuracy and computational time, a convergence analysis is required.

The new position of the crack front after each step is calculated on the basis of the SIF values for each front node. The maximum increment is given to the nodes with the higher equivalent SIF value. The displacement is a function of the SIF value all over the crack front. The increment to be assigned to a certain node is the maximum value multiplied by the ratio defined above.

On the basis of a predefined FCG law and the SIFs' values, the crack extension at each node of the crack front is computed. At the finale stage, the crack length and the corresponding number of cycles based on the SIF values allows to generate the a-N propagation curve and the corresponding residual life of the component.

3.2 Determination of Stress Intensity Factor

Different methods to determine the stress intensity factors (SIFs) are suggested in literature. Under the linear elastic fracture mechanics (LEFM), the most general method is the one which allows to calculate the stress intensity factor values once the value of the "J-integral" is known [12]. This latter is based on the use of an integral along a contour with which the strain energy release rate is computed. It is well known that the accuracy of such approach is limited by the approximation associated with the FE analysis. As a matter of fact, it is well known that in a context of finite element implementation the use of volumetric integrals leads to more accurate and reliable results in comparison with the calculation of integrals along a definite path, thanks to the introduction of biaxial and triaxial stress factors [13]. On the basis of this latter advantage, a numerical method for

the calculation of the SIFs through the use of a volumetric integral known as “M-Integral” [14] is used in the present paper. Yau et. al. [15] were the first to develop a formulation of the M-integral which allowed to obtain the SIFs related to the three modes of crack propagation. The formulation of the M-integral derives from the one related to the Rice’s method. The expression in terms of the displacement field around the crack tip allows to determine the kink angle, which is defined as the angle between the direction along which the crack front will diverge and the direction of the propagation related to the previous crack grow step. This latter is measured in a plane which is perpendicular to the crack front and the crack surface.

3.3 Kink Angle

There are different criteria used to calculate the kink angle. One of the most popular is the one formulated by Erdogan and Sih [16], which identifies the progress direction of the crack with the direction coinciding to the maximum value of the $\sigma_{\theta\theta}$ circumferential stress. The crack growth is directly determined by the local stress field along a small circle having an r radius centred at the crack tip. For isotropic materials, the hoop stress is related to the resolved mode I stress intensity factor, K_I^r, by the relation:

$$K_I^r(\theta) = \sigma_{\theta\theta}\sqrt{2\pi r} = \cos\frac{\theta}{2}\left[K_I cos^2\frac{\theta}{2} - \frac{3}{2}K_{II}\sin\theta\right] \quad (1)$$

If an isotropic material toughness is specified, a numerical algorithm is used to find the θ angle that maximises K_I^r.

3.4 Equivalent SIF range

In most real cases there is a simultaneous presence of the three modes. It is therefore necessary to consider the equivalent value of the ΔK, ΔK_{eq}, which is the value to predict the propagation of a mixed mode fatigue crack. Different formulae have been proposed to obtain the value of the ΔK_{eq}. Eqn. (2) is used in this paper, which combines the SIFs values through the use of the mixity factors

β_{II} and β_{III} [17]. Such factors are given by the ratio between the fracture toughness in mode II and mode III in relation to mode I (K_{IC}), namely, $\beta_{II} = K_{IIC}/K_{IC}$, $\beta_{III} = K_{IIIC}/K_{IC}$.

$$\Delta K_{eq} = K_{eq,max} - K_{eq,min} \tag{2}$$

$$\begin{aligned} K_{eq,max} &= \sqrt{K_{I,max}^2 + \left(\beta_{II} K_{II,max}\right)^2 + \left(\beta_{III} K_{III,max}\right)^2} \\ K_{eq,min} &= \sqrt{K_{I,min}^2 + \left(\beta_{II} K_{II,min}\right)^2 + \left(\beta_{III} K_{III,min}\right)^2} \end{aligned} \tag{3}$$

3.5 Fatigue Crack Growth Model

Among the different analytical models to approximate the sigmoidal curve, the most commonly used is the Paris' law [17]. However, on one hand the analytical formulation of the Paris law is very simple, making it widely adopted in industrial applications, on the other hand it is well known [18] that Paris Law is only applicable for the Paris regime and needs to be modified for the prediction of crack growth in the near threshold regime and the fast crack growth regime. In an attempt to overcome this problem, different FCG models [18] were proposed in literature, characterized by an increasing number of parameters to describe in the most accurate way the propagation sigmoid observed experimentally.

The NASGRO equation [19-21] can mathematically represent all the three propagation regions, including also the effect of the mean stress and the crack closure. The mathematical representation of the NASGRO equation is:

$$\frac{da}{dN} = C\left(\left(\frac{1-f}{1-R}\right)\Delta K\right)^n \frac{\left(1-\frac{\Delta K_{Th}}{\Delta K}\right)^p}{\left(1-\frac{K_{max}}{K_C}\right)^q} \tag{4}$$

where, a is crack length, N is number of load cycles, C, n, p, q are empirical coefficients, R is the stress ratio, ΔK is the stress-intensity factor (SIF) range, ΔK_{th} is the threshold of SIF, K_{max} is the SIF of

the maximum loading force in the cycle, and K_c is critical value of SIF referred to fracture toughness. f denotes Newman's function describing crack closure[20, 22].

4. FE MODEL

The H-shaped specimen has the shape and geometry shown in Figure 3.

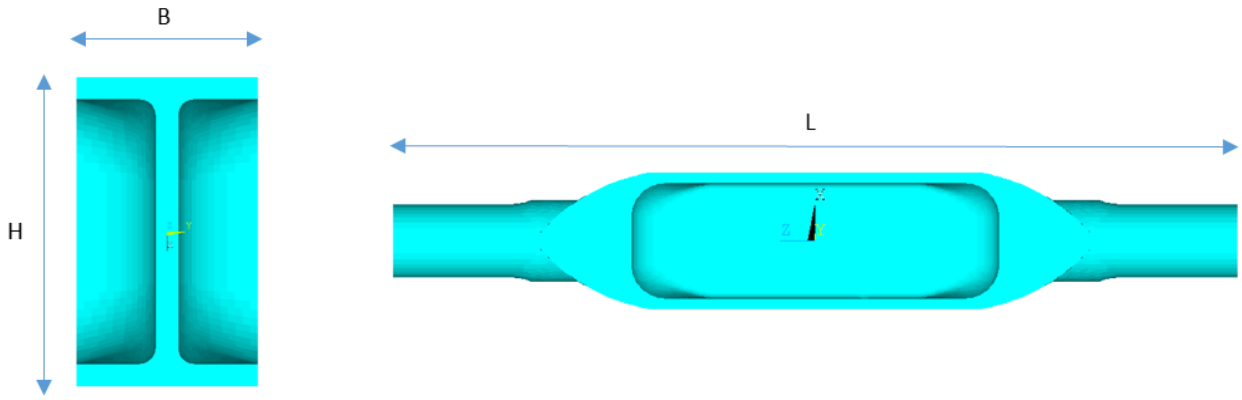

Figure 3 Geometry of the Specimen and main dimensions.

Through the use of commercial software ANSYS® R16.1, the FE model of the uncracked specimen was established by using 8-nodes Solid 185 elements with linear shape function.

The values of the main dimensions of the specimen together with the material properties related to the aluminium alloy F357 are reported in Table 2. The thickness of the web and flange is identical.

Table 2 Specimen dimensions and F357 properties

YS [MPa]	E [MPa]	K_{IC} [MPa√mm]	L [mm]	H [mm]	B [mm]	t [mm]
300	71000	1042	350	56	33	4

The Nasgro equation is used as fatigue crack growth model. In order to completely define this propagation model, the values of all constants are needed. These are obtained through experimental tests on standard specimens. Table 3 reports the values of all constants of the material related to the Nasgro model. It should be noted that a_0 is not the initial crack length in the model.

It is the intrinsic crack length used in NASGRO equation associated with the crack growth threshold. The recommended value for a_0 is 0.0381mm (0.0015inch) and has been used in this paper [23].

Table 3 Nasgro Constants (Units are N, mm, MPa√mm, mm/cycle)

C	n	p	q	K_{th}	C_{th+}	C_{th-}	α	S_{max}/S_{Flow}	$a_{\_o}$	A_k	B_k
3.0447e-11	2.54	0.28	2.0	38.54	1.85	-0.36	2	0.3	0.0381	1	0.25

The position of the nucleation area with regard to the specimen cross-section is shown in Fig. 4 based on the analysis of the fractographic evidence. The initial characteristic dimension of the defect is set equal to 1 mm. By means of the software FRANC3D®, a crack having an initial semi-circular shape with a radius of 0.5 was inserted in the uncracked model.

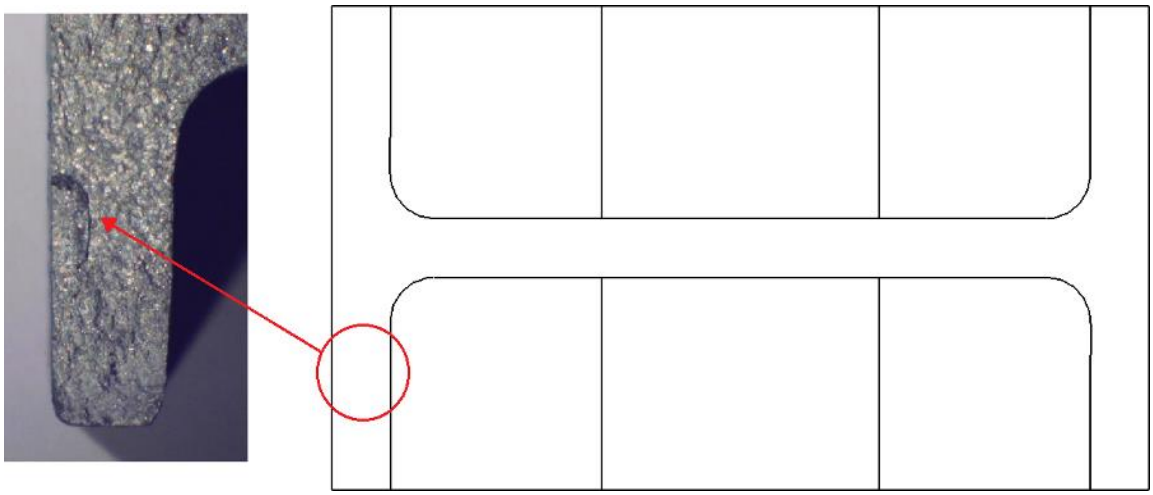

Figure 4 Position of the defect within the considered specimen

To optimize the computational cost associated with the process, part of the entire specimen, shown in figure 5 as local, has been selected and imported in FRANC3D®. The local model is remeshed every step keeping fixed the external position of the nodes. In this way, the remaining part of the model together with the boundary conditions is attached to the local model and solved every step without changing its discretization. As a consequence, the number of elements and nodes of the full model doesn't increase too much.

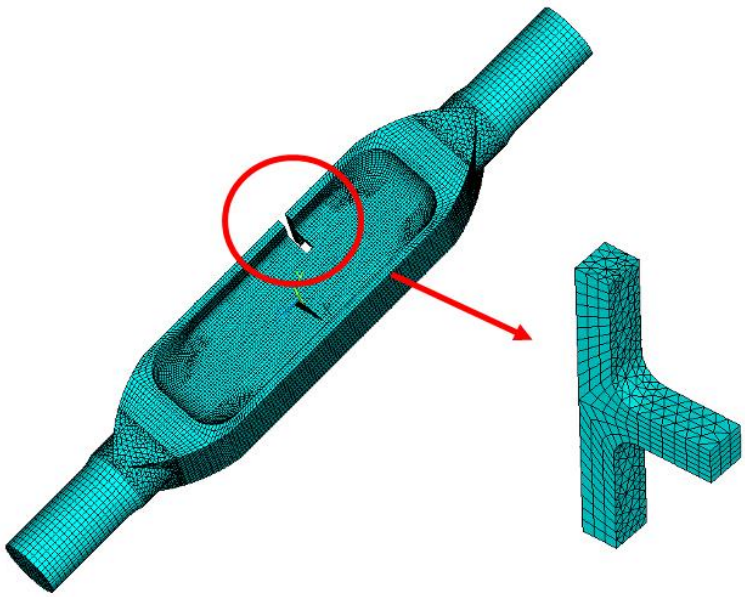

Figure 5 – Position of the local model in respect to the entire model.

In order to identify the effects associated with the inclination of the crack in respect to the applied load, three different configurations have been considered in which the initial position of the crack is such that it is inclined in respect to the horizontal plane of an angle equal to 0^o, 30^o and 45^o. These configurations correspond to 90^o, 60^o and 45^o in respect to the line along which the load is applied (Fig. 6).

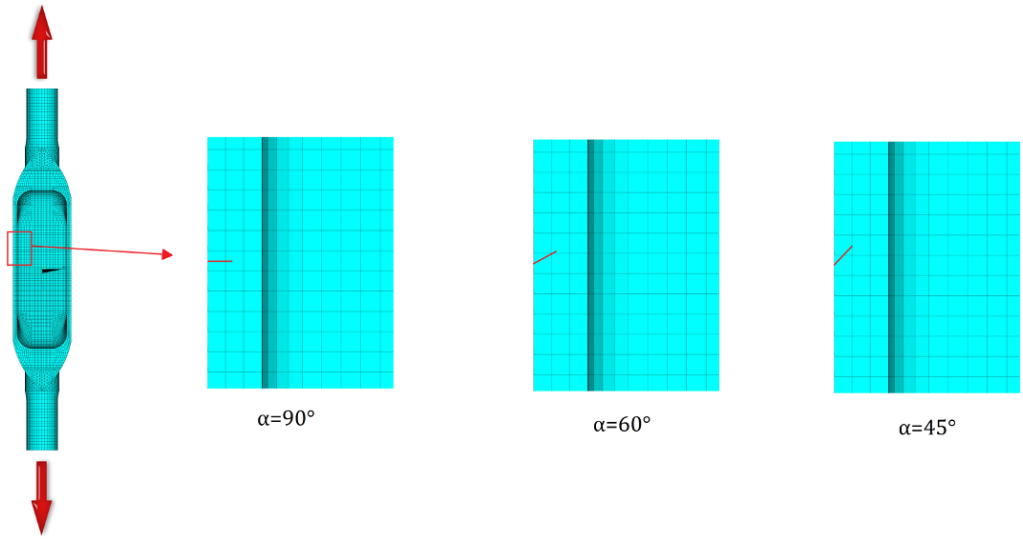

Figure 6 Orientation of the Initial defect.

The maximum circumferential tensile stress criterion is used to predict the crack propagation angle. On the basis of the convergence analysis, the optimal increment of the crack front Δa was set equal to 0.05mm. Through convergence, the result is made independent from the value of the Δa in terms of fatigue life. By setting an average increment equal to 0.05 mm, the propagation analysis was made by performing a total of 76 steps. The model with the crack having a given length is solved and the SIF's values together with the crack growth extension are derived. The new crack is inserted in the model and the new cracked model is built. The process is repeated until the failure criterion set in terms of either critical crack length or critical SIF value is reached.

For each step the SIF corresponding to the three modes together with the geometry of the crack front is stored.

5. Results and Discussion

5.1. Finite Element Model Validation

The validation of the numerical model implemented in ANSYS has been performed using the experimental results acquired during the experimental campaign on the H shape samples. The fatigue test data available refers to a crack at 90^{o} to the loading direction and for that reason the comparison is performed for that particular configuration. The load-direction stress under the maximum applied load is shown in Fig. 7. The stress value reached in the cross-section where the crack has been inserted and the propagation has been simulated is 180 MPa. The fatigue life predicted by the FE simulation is 109309 cycles.

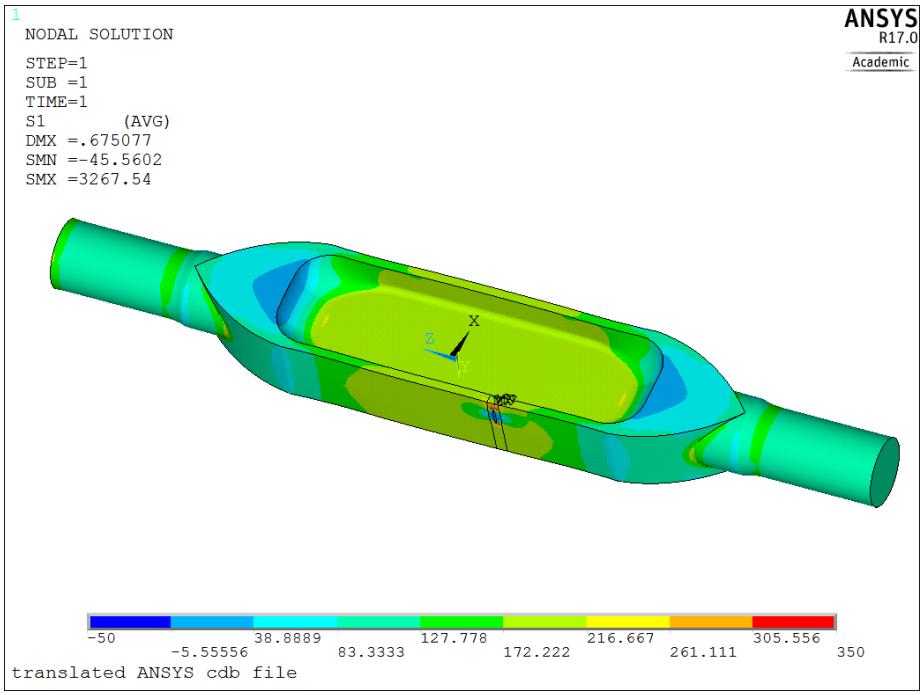

Figure 7 - Contour plot of the load direction stress.

The curve in figure 8 is the experimental data of fatigue life versus the fatigue stress under the maximum applied fatigue load. The fatigue life determined by the test data in Fig. 8 is 10^5 cycles. Compared with the 109309 cycles predicted in the FE simulation, the difference between the numerical and the experimental results is 8.5%

Figure 8 - Experimental results (line) [10] and numerical result (square symbol)

5.2. Mixed Mode Crack Growth Behaviour

For each crack inclination the SIFs values along the fronts have been determined. The variation of SIF values with the crack length for the first modes are shown in Fig. 9. The values shown in the graphs refer to three positions A, B, and C along the front (Fig. 10), namely 0.2 0.5 0.8, identified by means of a non-dimensional curvilinear coordinate system shown in Fig.10. As shown in Fig. 9, the difference is mainly related to the first phase of the crack propagation, during which the surface of the crack rotates and becomes perpendicular to the loading direction.

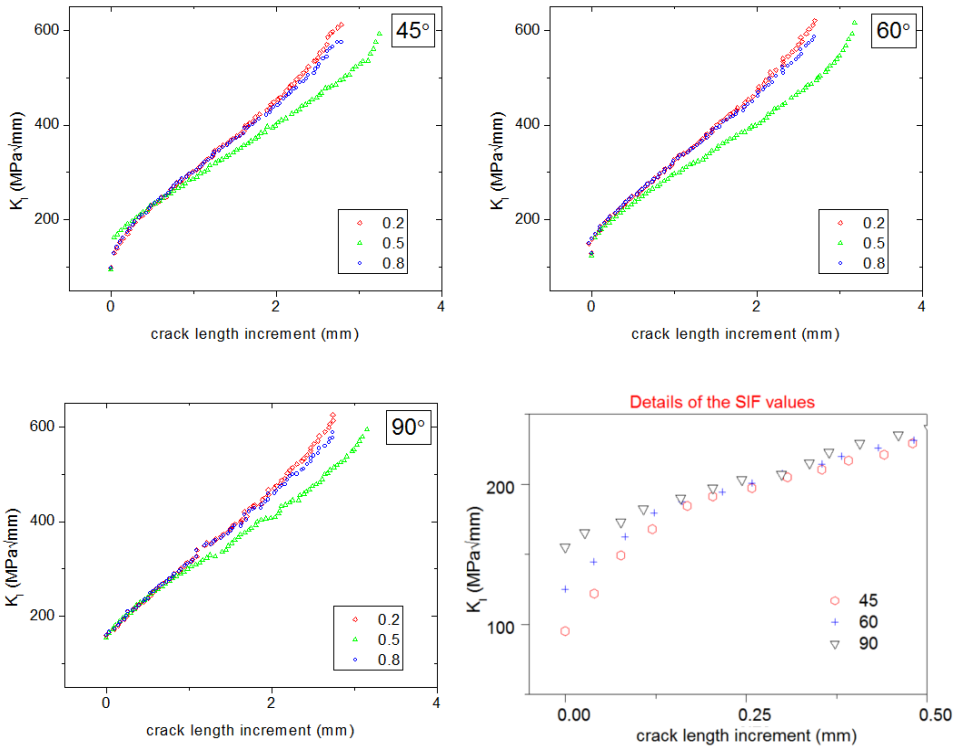

Figure 9 - K_I vs crack length increment under three crack orientations: a) 45° b) 60° c) 90° and detail of the first propagation stage up to 0.5 mm d)

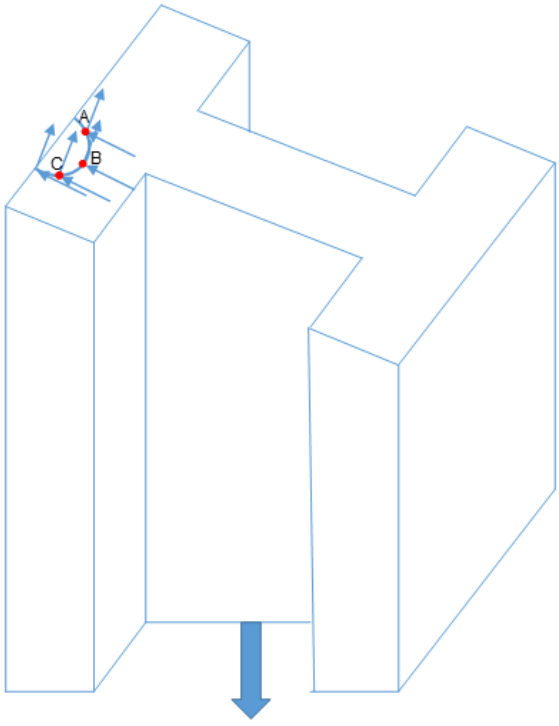

Figure 10 - illustration of mixed mode loading at different locations of the crack front when the crack face is not perpendicular to the loading direction

When the crack is initially set with an inclined angles α equal to 60° and 45°, the values of the K_{III} are not negligible, due to the resolved shear stresses acting on the crack face as shown in Fig.10. Moreover, the value of the K_I is lower than the case in which the crack is set perpendicular, due to the reduction of the value of the normal stress component to the fracture surface. All this can also be represented through the value of the K_{III}/K_I mode mixity parameter, which quantify at a given location along the front the contribution of mode III to the crack propagation [24, 25]. The variations of K_{III}/K_I for the nodes at the normalized coordinate 0.2 and 0.8 at different crack inclination α=90°, α=60°and α=45° are shown in Fig. 11.

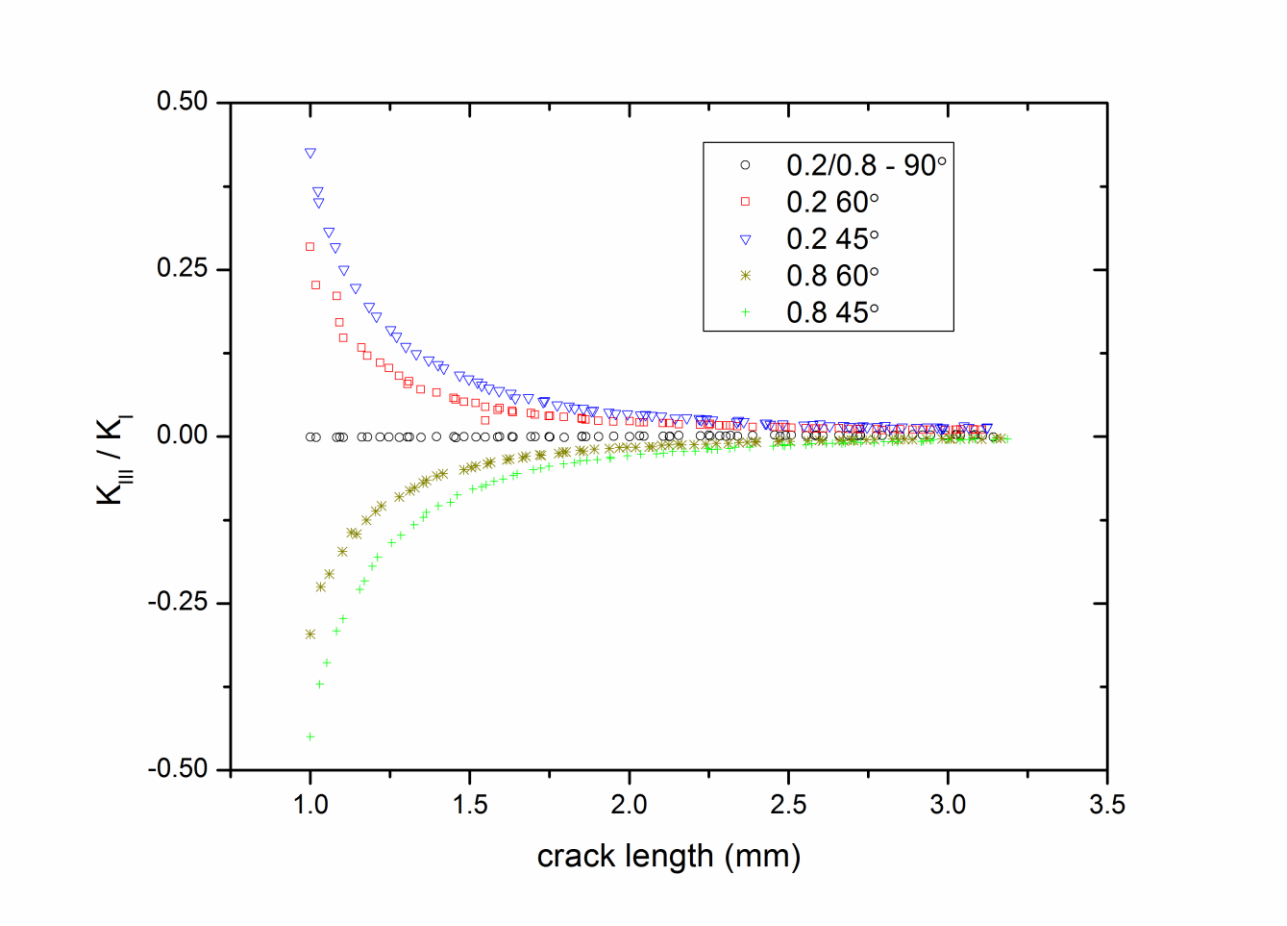

Figure 11 - KIII/KI variations for different inclination at two position along the crack front.

The first half millimetre of the crack propagation process is characterized by high values of the K_{III} at the two ends of the crack front corresponding to 0.2 and 0.8. The equivalent SIF range will be higher and so will be the values of the crack growth rate. As a consequence the parts of the front in

correspondence of the two ends will propagate more with a change in the shape of the crack front from circular to elliptical. Due to the different rate with which the ratio decreases at 0.2 in respect to 0.8, the crack growth rate will be different at the two ends having an elliptical shape as shown in Fig. 12.

In all cases the part of the fronts opposite to the web is characterized by a more extension with a front which is not symmetric in respect to the centre of the initial defect due to the higher FCG rate. The different condition related to the shorter ligament towards the edge of the flange is also responsible for the higher crack growth rate.

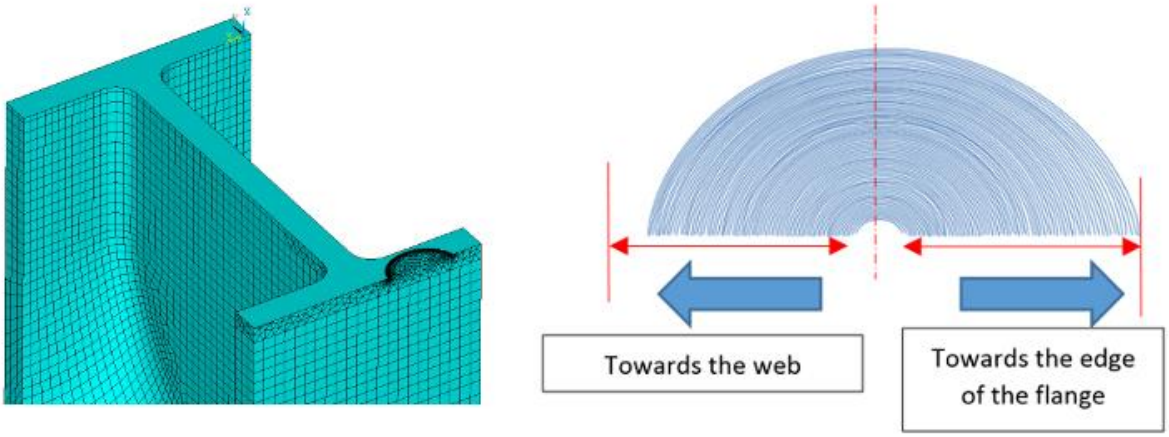

Figure 12 - Propagation of the crack fronts through the flange.

The evolution of the SIFs values related to the mode III can also be explained by means of the contour plots shown in Fig. 13 A and B. The shear stress is responsible for the mode II at the centre and the III mode at the two ends of the crack front, respectively. The plastic constraint is less approaching the external surface. That's the reason why in the centre the SIF values related to the II mode are quite low compared to the opening mode. At the two ends the deformation is higher due to the less constraint and the SIF values related to the mode III are higher. Approaching the end of the propagation phase, the maximum value of the K_{III} SIF moves to the centre of the crack front and it is reached at 60^{o}. This is due to the fact that the final stage considered for the contour plots is the one just before the crack completely penetrates the entire thickness. Since the material ahead

the crack tip is small the component can locally deform more compared to the two ends of the crack front.

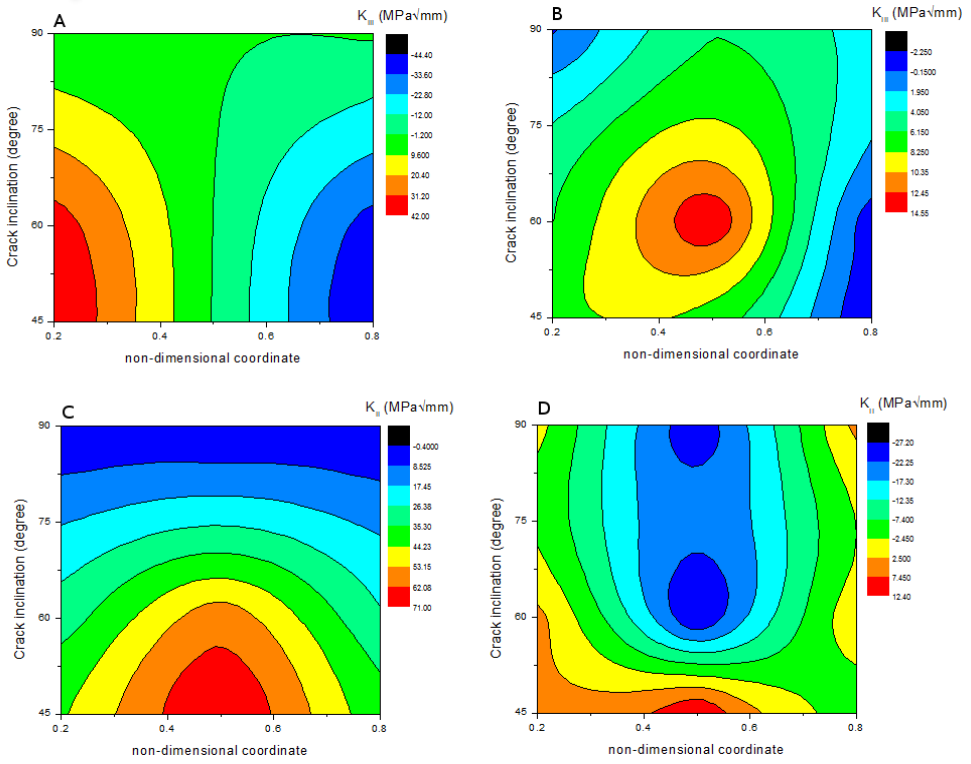

Figure 13 - Contour plot reporting the KIII values at the beginning (A) and the end (B) of the considered propagation phase, and KII values at the beginning (C) and at the end (D) of the considered propagation phase.

The K_{II} SIF values in correspondence of the initial step of the propagation process in the centre of the crack front is higher than those related to the third mode and computed at the two ends (Fig. 13 C and D). These higher values are associated to the rotation of the crack surface. The shear stress associated to the II mode affect the direction along which the principal stress acts and as a consequence the direction along which the crack grows. Having used the maximum circumferential tensile stress criterion to identify the kink angle the concurrent effects of the mode I and mode II produce a variation in the rotation of the fracture surface.

The variation in the inclination of the crack can also be seen in terms of displacements of the central node of the front during the propagation phase for the three configurations in the plane normal to

the crack front. In particular (Fig. 14) the path followed by the central nodes in the plane orthogonal to the crack front is shown.

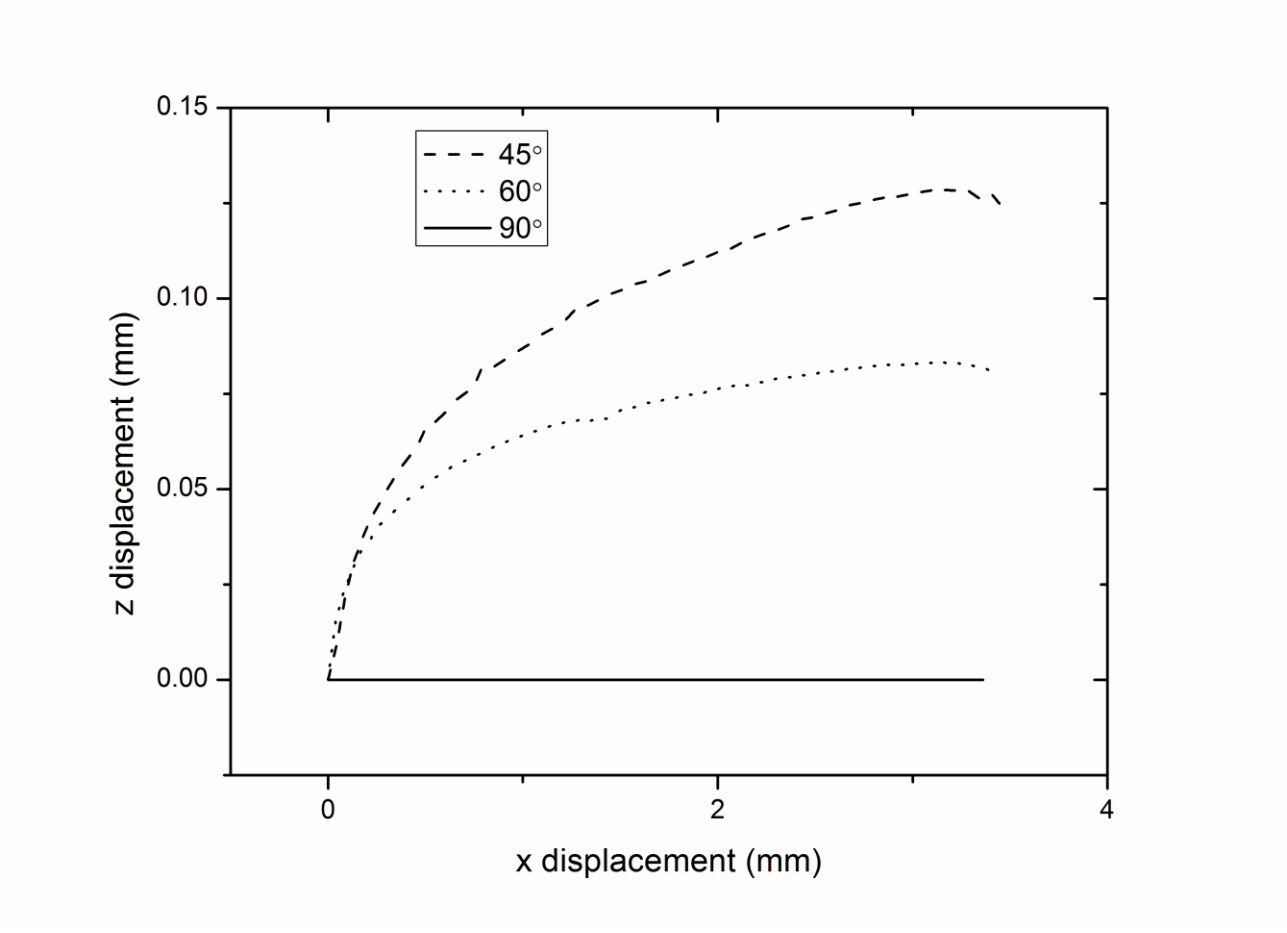

Figure 14 - Path followed by the central node of the front at different initial inclination value

The fracture surfaces for the three crack inclination considered in this paper, in correspondence of the last crack front before the crack would completely pass through the flange are reported in Fig. 15. In particular, it can be seen that the crack initially inclined deviates from the inclined plane becoming planar.

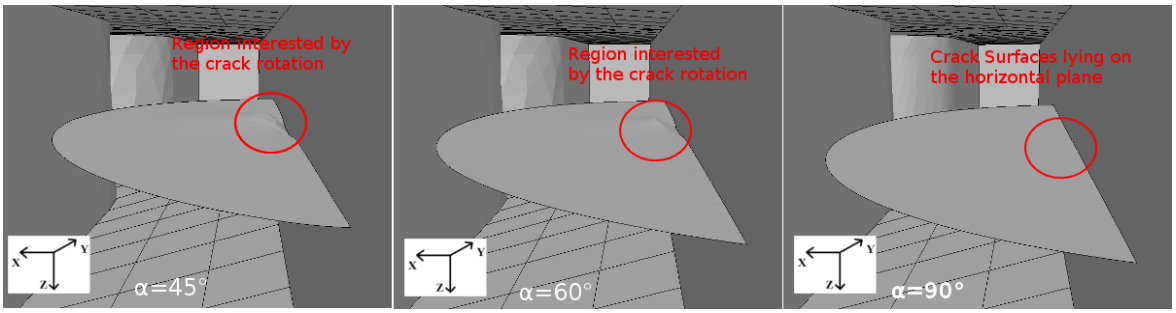

Figure 15 - Fracture surfaces in the flange for different inclinations.

The evolutions of the K_{III} as a function of K_I during the crack propagation are shown in Fig. 16 for the three inclination at the three positions on the crack front. The maximum values of the K_{III} are at the two ends of the crack front when the initial crack face is 45° to the loading direction, which is expected as the resolved shear stress reaches the maximum under the same axial loading. It is worth noting that Fig.17b) represents the K_{III} value at the mid-point of the crack front, which is zero at the beginning of the crack propagation regardless of the crack orientation. K_{III} component at this position will develop during the crack propagation as the crack growth rate towards the edge of the flange is different to the growth rate towards the web as shown in Fig.12. Fig.17a) and Fig.17c) are for the crack front locations having large K_{III} components for the inclined cracks (45° and 60°) and hence are different to the trend in Fig.17b).

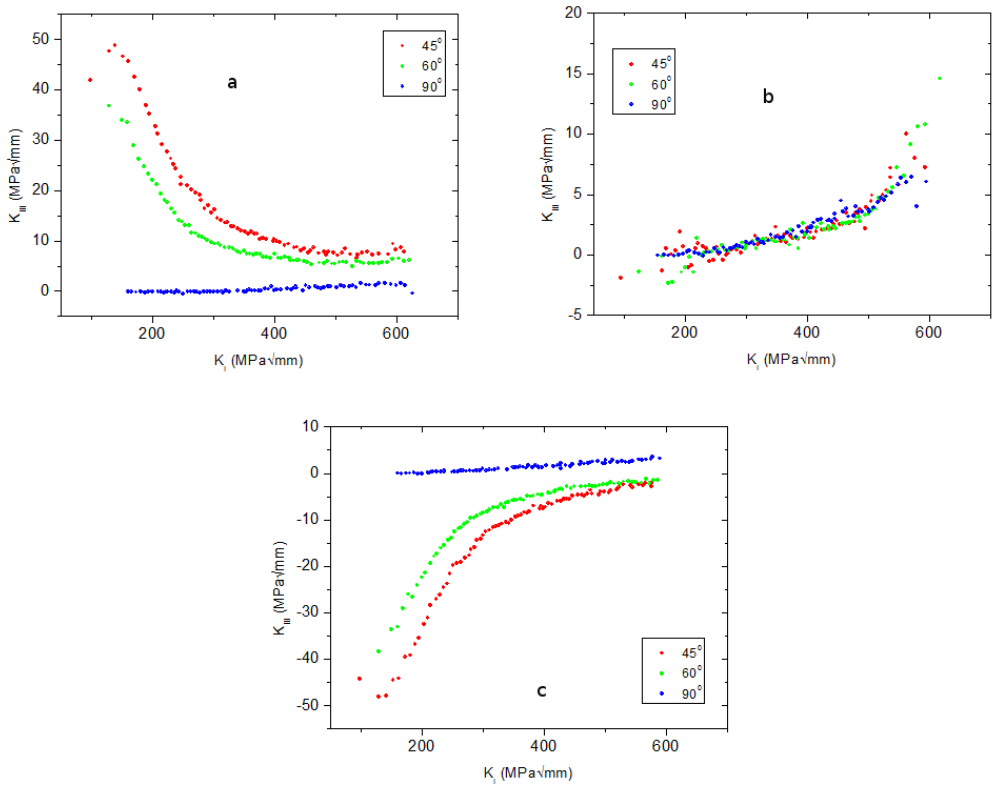

Figure 16 K_{III} vs K_I during crack propagation for positions on crack front: a) position A, b) position B, c) position C

In order to predict the fatigue life of the component it is necessary to determine the evolution of the equivalent SIF range ΔK_{eq} and the corresponding crack length estimated along a particular

"path". The chosen path is the one that maximize the values of the stress intensification factors. In the expression of the ΔK_{eq} the K_{II} and K_{III} stresses intensification factors are considered through the use of both mixed mode coefficients β_{II} and β_{III}.

The mixed mode coefficients are defined as the ratio between the fracture toughness under pure mode I and that under pure mode II. This ratio is a measure of the contribution of each mode to the failure condition. For the particular alloy studied in the present paper the fracture toughness under pure mode II is not available. For this reason, the values reported in literature for aluminium alloy was used [26].

From the analysis of the crack fronts obtained with the proposed numerical model it can be observed that in the case in which the crack was initially perpendicular to loading line, the propagation is planar along the whole curvilinear crack front, which is expected as the crack is under pure mode I loading. In the case of an inclined crack, as shown by Shlyannikov et al [27] the value of the kink angle varies along the crack front. In fact, given the variation of the relative contribution from mode II along the front, the value of this angle will have to vary from point to point of the front. Cracks which were initially set at 60° and at 45° tend, during the propagation phase, to rotate and set themselves perpendicular to the load direction. The kink angle, which is computed using Eqn. 1, is a function of $\sigma_{\theta\theta}$ that acts along a direction that varies during the propagation phase due to the decrease of the shear stress. Therefore, the contribution of the K_{III} and K_{II} will decrease after a certain number of steps.

Moreover, in all cases it can be observed that the crack grow rate varies along the front. This behaviour is mainly due to the reduced ligament, that is to say the little portion of the material which opposes to these fronts propagation and therefore to the increase of the crack growth rate.

A further evidence to illustrate the presence of the mode III is the displacement field close to the crack front. It can be observed that, as shown in Fig. 17, the material at the left side of the crack surface is

subject to a downward movement in y direction (the blue colour represents the negative y displacement), while the material at the right side is subject to an upward movement (the red colour represents the positive y displacement). These differential displacements in the plane of the crack surface towards the y direction is the proof of the mixed mode effect.

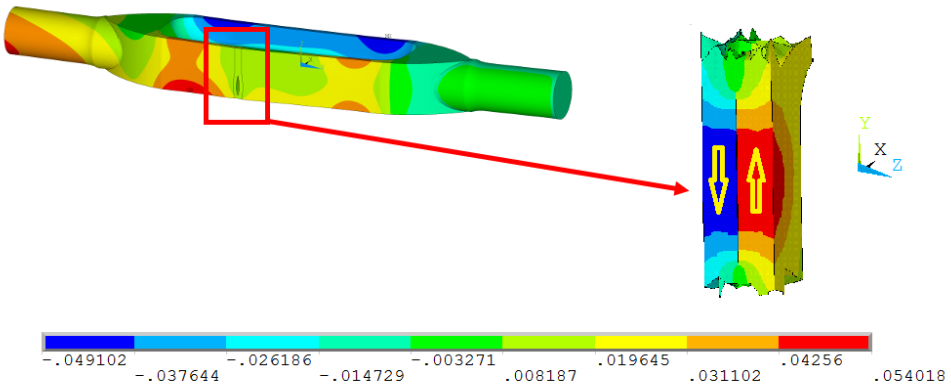

Figure 17 - Displacement field in millimetre.

As shown in Fig.18, there is a split in the crack front when the crack becomes a through-thickness crack. The front which is growing toward the web has a different condition in terms of triaxiality which turns in a different fatigue crack growth behaviour. In particular, the crack growth rate towards the web is greater than that on the opposite side of the front propagating towards the toe.

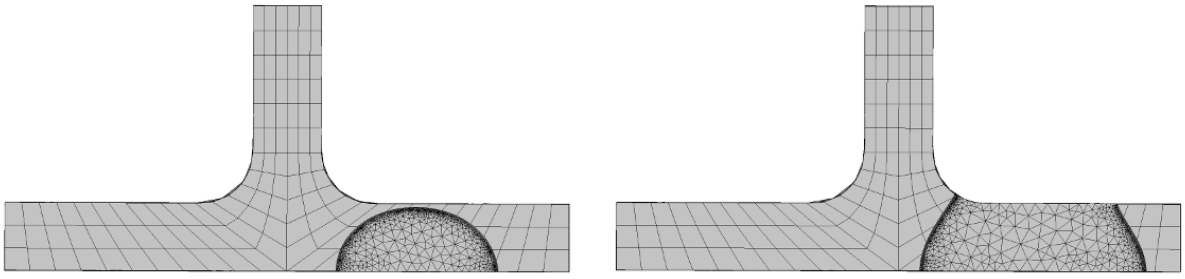

Figure 18 - Fracture surface before (left) and after (right) the crack passes through the thickness

Fig. 19 shows the a-N curves obtained through the integration of the model equation for cracks under three different orientations. A duration of the whole propagation phase equal to N=109309 cycles is obtained when the crack is perpendicular to the loading direction.

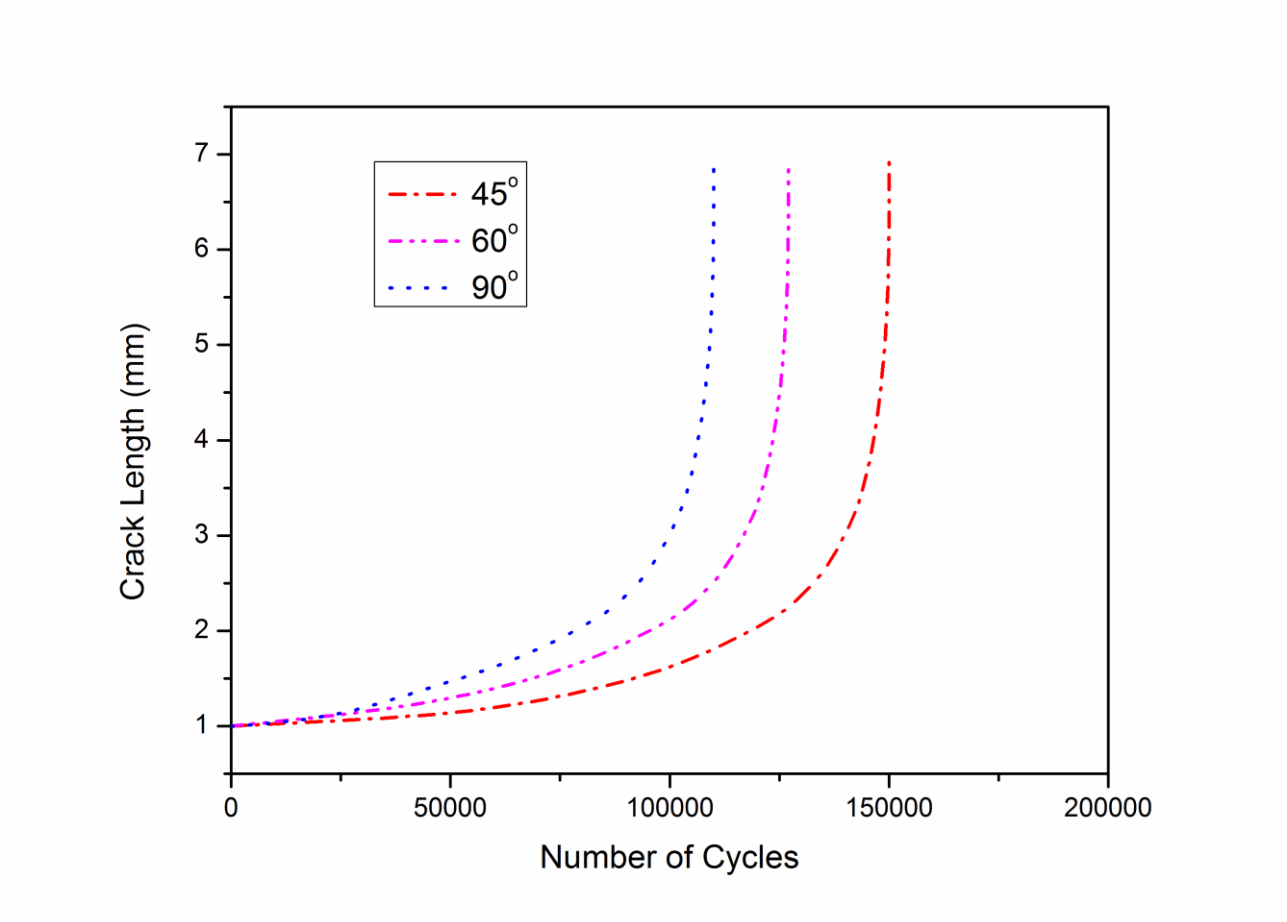

Figure 19 – a-N curves obtained for the three different orientations.

The value of the duration of the propagation phase related to the crack where α=60° is equal to N=126796 cycles, while the value in the case where α=45° is equal to N=149792 cycles. It can be observed that under the same tensile load, the lower the initial inclination of the crack with regards to the direction of applied load and the longer the fatigue life. When α=60° there is an increase of 14% of the duration compared with the case of the crack perpendicular to the load. If α=45° the increase is equal to 15% with regard to the case in which α=60°, and of 27% with regards to the case of a perpendicular crack.

6. CONCLUSIONS

This paper presents a numerical study of mixed mode crack growth behaviour of defects in aluminium F357 alloy manufactured by foundry. Following conclusions can be drawn based on the numerical results obtained:

- The initial phase of the mixed mode fatigue crack growth is characterized by the presence of the maximum mode III SIF at the two ends of the crack front and the maximum mode II SIF at the middle of the crack front. They interact with the mode I SIF and cause the rotation of the crack surface making the final crack orientation perpendicular to the loading direction.
- The central part of the crack front grows faster than the two ends of the crack front due to the fact that the central part is under the action of lower values of K_I and the two ends of the crack front interact with the free surface. This changes the crack shape from the initial circular shape to the final elliptical shape.
- Out of the three crack orientations analysed in the paper, the crack at 45° to the loading direction has the longest fatigue life. It is 15% greater than that of the crack at 60° to the loading direction and 27% greater than that of the crack perpendicular to the loading direction.

7. Acknowledgment

The Authors wish to thank Claudio Di Gregorio – Leonardo Helicopters S.P.A. for the support provided during the experimental activities and the use of some of the experimental results for the preparation of this paper.

8. References

1. Plumtree, A. and S. Schafer. *Initiation and short crack behaviour in aluminium alloy castings*. in *EGF1*. 2013.
2. Mo, D.-F., et al., *Crack initiation and propagation of cast A356 aluminum alloy under multi-axial cyclic loadings.* International Journal of Fatigue, 2008. **30**(10): p. 1843-1850.
3. Timelli, G. and F. Bonollo, *Quality mapping of aluminium alloy diecastings.* Metallurgical Science and Tecnology, 2013. **26**(1).
4. Avalle, M., et al., *Static and fatigue strength of a die-cast aluminium alloy under different feeding conditions.* Proceedings of the Institution of Mechanical Engineers, Part L: Journal of Materials Design and Applications, 2002. **216**(1): p. 25-30.
5. Burton, C., et al., *Failure Analysis of a Cast A380 Aluminum Alloy Casting Using a Microstructurally Based Fatigue Model.* TRANSACTIONS-AMERICAN FOUNDRYMENS SOCIETY, 2006. **114**: p. 97.

6. Ceschini, L., et al., *Room and high temperature fatigue behaviour of the A354 and C355 (Al–Si–Cu–Mg) alloys: Role of microstructure and heat treatment.* Materials Science and Engineering: A, 2016. **653**: p. 129-138.
7. Aufderheide, R., et al., *Eliminating Fish-Eye Defects in Ductile Castings.* TRANSACTIONS-AMERICAN FOUNDRYMENS SOCIETY, 2002. **2**: p. 917-928.
8. TROJAN, P.K., *Inclusion Forming Reactions.* 1988.
9. Dietrich, L. and J. Radziejewska, *The fatigue damage development in a cast Al–Si–Cu alloy.* Materials & Design, 2011. **32**(1): p. 322-329.
10. Westland, A., *Caratterizzazione a fatica assiale di provini ad H fusi in terra da AW Benevento in lega AL F357 T6 Anodizzati.* Internal Report 3084, 2014.
11. Bittencourt, T., et al., *Quasi-automatic simulation of crack propagation for 2D LEFM problems.* Engineering Fracture Mechanics, 1996. **55**(2): p. 321-334.
12. Rice, J.R., *A path independent integral and the approximate analysis of strain concentration by notches and cracks.* Journal of applied mechanics, 1968. **35**(2): p. 379-386.
13. Rao, B. and S. Rahman, *An interaction integral method for analysis of cracks in orthotropic functionally graded materials.* Computational mechanics, 2003. **32**(1-2): p. 40-51.
14. Moran, B. and C. Shih, *Crack tip and associated domain integrals from momentum and energy balance.* Engineering fracture mechanics, 1987. **27**(6): p. 615-642.
15. Yau, J., S. Wang, and H. Corten, *A mixed-mode crack analysis of isotropic solids using conservation laws of elasticity.* Journal of Applied Mechanics, 1980. **47**(2): p. 335-341.
16. Erdogan, F. and G. Sih, *On the crack extension in plates under plane loading and transverse shear.* Journal of basic engineering, 1963. **85**(4): p. 519-525.
17. Paris, P. and F. Erdogan, *A critical analysis of crack propagation laws.* Journal of basic engineering, 1963. **85**(4): p. 528-533.
18. Schijve, J., *Fatigue of structures and materials*. 2001: Springer.
19. Newman, J., *A crack-closure model for predicting fatigue crack growth under aircraft spectrum loading*, in *Methods and models for predicting fatigue crack growth under random loading*. 1981, ASTM International.
20. Newman, J.J., *A crack opening stress equation for fatigue crack growth.* International Journal of fracture, 1984. **24**(4): p. R131-R135.
21. Forman, R., *Study of fatigue crack initiation from flaws using fracture mechanics theory.* Engineering Fracture Mechanics, 1972. **4**(2): p. 333-345.
22. Wu, X., M. Chi, and H. Gao, *Damage tolerances of a railway axle in the presence of wheel polygonalizations.* Engineering Failure Analysis, 2016. **66**: p. 44-59.
23. Forman RG, Shivakumar V, Cardinal JW, Williams LC, McKeighan PC. *Fatigue crack growth data base for damage tolerance analysis*, DOT/FAA/AR-05/15; August 2005.
24. Wei, L.-W. and M. James, *Fatigue crack closure for inclined and kinked cracks.* International journal of fracture, 2002. **116**(1): p. 25-50.
25. Chow, W. and S. Atluri, *Fracture and fatigue analysis of curved or kinked cracks near fastener holes.* Finite elements in analysis and design, 1996. **23**(2): p. 91-100.
26. Richard, H., B. Schramm, and N.-H. Schirmeisen, *Cracks on mixed mode loading–theories, experiments, simulations.* International Journal of Fatigue, 2014. **62**: p. 93-103.
27. Shlyannikov, V., A. Tumanov, and S.Y. Kislova. *Effects of biaxial loading on inclined surface cracks behavior*. in *ICMFF9*. 2013.